Pilot study on the Application of Photothermal Therapy to Eliminate Melanoma Cancer Cells in a Murine Melanoma Model

Javier Domingo-Diez[1]; Óscar Casanova-Carvajal[1,2,3]; Lorena Marrodán[1]; José Javier Serrano-Olmedo[1,3,4]; Milagros Ramos-Gomez[1,3,4]

[1]*Universidad Politécnica de Madrid - (ES), España; javier.domingo@ct.upm.es, oscar.casanova@ctb.upm.es, l.marrodan@upm.es, josejavier.serrano@upm.es, milagros.ramos@ctb.upm.es*

[2]*Departamento Ingeniería Eléctrica, Electrónica, Automática y Física Aplicada, Escuela Técnica Superior de Ingeniería y Diseño Industrial ETSIDI, Universidad Politécnica de Madrid, 28040 Madrid, Spain;*

[3]*Centro de Investigación Biomédica en Red para Bioingeniería, Biomateriales y Nanomedicina, Instituto de Salud Carlos III, 28029 Madrid, Spain;*

[4]*Departamento de Tecnología Fotónica y Bioingeniería, ETSI Telecomunicaciones, Universidad Politécnica de Madrid, 28040 Madrid, Spain;*

***Abstract*– Melanoma is an aggressive cancer with high metastatic potential and limited treatment options. This study evaluates Photothermal Therapy (PTT) using gold nanorods (GNRs) in a murine melanoma model. Tumors treated with PEG-functionalized GNRs and irradiated with an 808 nm laser showed complete elimination in small tumors (≤2 mm) and a 45% reduction in growth rate for larger tumors. The results confirm that PTT is effective for early-stage melanoma, but larger tumors require additional strategies, highlighting its potential as a minimally invasive, targeted therapy with future clinical applications.**

Keywords: Melanoma, Photothermal Therapy, Gold Nanorods, Nanomedicine, Tumor Regression.

I. INTRODUCTION

Melanoma is the cancer with the greatest metastatic potential of any solid tumor. Cutaneous melanoma arises from malignant transformation of melanin-producing melanocytes in the cutaneous basal epidermis [1]. In contrast, noncutaneous melanoma arises from the same transformation of melanocytes in the uvea [2], gastrointestinal tract [3], genitalia and urinary tract [4], and meninges [5].

As for cutaneous melanoma, it is an aggressive and invasive cancer of the skin that accounts for 1.7% of all cancers in the world population and ranks 15th among all common cancers worldwide. The incidence of melanoma continues to increase with age, with new cases being reported in the 65-74 age group, with the average melanoma case being diagnosed at age 64. Gender-related incidence is more common in women at an early age, while in men it is more prevalent from the age of 55 [6].

Most patients with early diagnosis of melanoma are in the early stages of tumor development, and the treatment to be followed is removal of the tumor by surgery with total removal without tumor recurrence. However, some patients with disseminated disease and late diagnosis account for 10% of melanoma cases with poor prognosis and probably low response to other treatment [7].

However, these treatments often lead to significant side effects. Due to the heterogeneous nature of cancer and the risks associated with current treatments, there is a need for the development of new therapeutic strategies. Innovative approaches, such as hyperthermia, are being explored and can be combined with conventional methods [8], [9].

Photothermal therapy (PTT) is a highly effective emerging non-invasive cancer treatment capable of selectively eliminating tumor cells by converting light irradiated by a laser of appropriate wavelength into heat by nanoparticles (NPs). The elevated temperature in the microenvironment directly affects cancer cells, triggering necrotic and apoptotic pathways. The extent of these pathways depends on the temperature reached during the irradiation procedure (typically ranging from 41–45 ºC) [10].

Gold nanorods (GNRs) are characterized by their remarkably high light-to-heat conversion efficiency, making them the most commonly used photothermal agents in PTT. The optical properties of GNRs are influenced by their size and shape. They are governed by the phenomenon of localized surface plasmon resonance (LSPR), which occurs when GNRs are exposed to light radiation, causing the plasmon to oscillate on the surface of the GNRs [11]. This unique feature of GNRs enables them to possess a remarkable capacity for photothermal conversion. Furthermore, GNRs can be biofunctionalized with biomolecules such as antibodies [12],

peptides [13], proteins [14], or nucleic acids [15] to specifically target tumor cells. Another widely used molecule for GNR biofunctionalization is polyethylene glycol (PEG), which prolongs the blood circulation time of GNRs and improves their biocompatibility [16]. When GNRs are not biofunctionalized with PEG, their surfaces are highly recognized by circulating blood plasma proteins, which can alter the properties of GNRs. This recognition often leads to aggregation, rendering GNRs less effective in PTT. In addition, another feature of GRNs in PTT is their accumulation in tumor tissue, called the enhanced permeation and retention effect (EPR). Massive irregular neovascularization in tumors with functional abnormalities in tumor vessels favors the EPR effect [17].

II. Material and Methods

A. Culture cell

Murine melanoma (B16F10) cells were kindly donated by Prof. Lisardo Bosca. Melanoma cell lines was maintained in DMEM (Gibco, Billings, MT, USA) supplemented with 10% heat-inactivated fetal bovine serum (FBS), 2 mM glutamine (Gibco, USA), 100 units/mL penicillin, and 100 g/mL streptomycin. Cell lines were maintained at 37 C in 5% CO2 and 95% air in a humidified atmosphere and passed twice a week to ensure their optimal growth.

B. PTT Device

A continuous-wave laser operating at 808 nm with a maximum output power of 5 W (fiber-coupled laser system, HJ Optronics, Inc., San Jose, CA, USA) was vertically connected to a collimator lens (F-C5S3-780, Newport Corporation, Irvine, CA,USA) through a one-meter-long multimode optical fiber with a core diameter of 600 m and a power transmission efficiency of 90–99% (Changchun New Industries, Changchun, China). The collimator was fixed to irradiate the tumors from the top in the *in vivo* studies. To determine the exact irradiation power, the fiber was connected to a power meter (PM USBLM-10, Coherent Inc., Santa Clara, CA, USA) using an SMA fiber adapter (PN 1098589, Coherent Inc., Santa Clara, CA, USA) and the software PowerMaxPC (Coherent Inc, Santa Clara, CA, USA).

C. Gold nanoparticles

The GNRs of different sizes with LSPR at 800 nm were prepared using as seeded-growth method with some modifications as described in [18]. Gold seeds. To prepare the growth solution, 9.111 g of CTAB (50 mM) and 870.5 mg (11 mM) of n-decanol were added to 500 mL of water and stirred at approximately 60 ºC for 30–60 min. The mixture was then cooled down to 30 ºC, and 250 L of a 0.05 M $HAuCl_4$ solution was added to 25 mL of the n-decanol/CTAB solution in a 50 mL glass beaker. The resulting mixture was stirred at 300 rpm for 5 min. Next, 125 L of a 0.1 M ascorbic acid solution was added, causing the orange-yellow solution to slowly turn colorless. At this point, a freshly prepared 20 mM $NaBH_4$ solution was injected (one shot) under stirring at 1000 rpm and 30 ºC. The injection resulted in brownish-yellow solutions, and the seed solutions were aged for at least 60 min at 30 C before use. It is important to note that the dimensions of the PTFE plain magnetic stirring bar (30 6 mm) used in the stirring process can strongly affect the quality of seeds. Synthesis of anisotropic seeds. In a typical synthesis, 1000 L of 0.05 M $HAuCl_4$, 800 L of 0.01 M $AgNO_3$,7mL of 1M HCl, and 1300 L of 0.1M ascorbic acid were added under vigorous stirring to 100 mL of a 50 mM CTAB and 13.5 mM n-decanol solution at exactly 25 C. Once the solution became colorless, 6 mL of the seed solution was added under stirring, and the mixture was left undisturbed for at least 4 h. The solution changed from colorless to dark-brownish gray, and the recorded longitudinal LSPR was located at 725–730 nm. The small anisotropic seeds were centrifuged at 14,000–15,000 rpm for 60 min in 2 tubes. The precipitate was collected, redispersed with 10 mL of a 10 mM CTAB solution, and centrifuged twice under the same conditions. The final Au0 concentration was fixed to 4.65 mM (Abs400 nm: 10; optical path of 1 cm).

Growth of this GNRs SGNRs. Briefly, in a typical synthesis, 3 mL of 0.01 M AgNO3, 1 mL of 0.05 M HauCl4, 3 mL of 1 M HCl, and 800 L of a 0.1 M ascorbic acid solution were added under stirring to 100 mL of a 50 mM CTAB and 11 mM n-decanol solution at 35 C. Next, 2500 L of the small anisotropic seed suspension was added under stirring. The mixture was left undisturbed for 4–6 h. The GNRs were forced to settle as sediment (by centrifugation at 8000 rpm, 30 min) to remove the excess of surfactant and redispersed in 10 mL of a 10mM CTAB solution (GNR stock solution). This procedure was repeated twice to remove n-decanol traces. The resulting GNRs presented an average length of 40 2nm and an average diameter of 10 ± 1nm.

Functionalization of GNRs. Typically, PEG-SH (15 mg) was added under stirring to 5 mL of a freshly prepared aqueous suspension of GNRs (2 mM of Au0, 1 mM CTAB). After 1 h, the excess of free PEG-SH was removed by one centrifugation cycle (8000 rpm, 30 min). Next, the precipitate was redispersed in 5 mL of 10 mM buffer (EBSS).

D. Melanoma tumor model

The experimental procedure to generate an animal model of melanoma based on the subcutaneous injection of B16F10 melanoma cells in immunocompetent C57/BL-6 mice is detailed. Subcutaneous injection is performed with 100,000 B16F10 cells in a total volume of 4 µL and tumor development is monitored for four days, at this time the tumor becomes evaluable using a digital caliper. Tumors are irradiated after local injection of GNRs (total volume of 4 µL at a concentration of 1.89 µg/mL, where the initial concentration of GNRs is 1.89 x 10^3 µg/mL and a 1:1000 dilution with PBS is performed) at a power of 450 mW for 25

minutes. The tumor is measured using an electronic caliper on different days evaluating the size over time, as well as its weight after removal, at the end of the experiment.

E. Statistical Analysis

The results are shown as the mean standard error of the mean from three to four experiments. The data were analyzed by single-factor analysis of variance followed by the post hoc Tukey's honestly-significant-difference test. A t-student was also performed to compare only two groups. A significant level of $p < 0.05$ was chosen. GraphPad Prism version 9 (GraphPad Prism Software, San Diego, CA, USA) was used for all statistical tests.

III. Results

A. Temporal evaluation of tumor size

Tumor implantation has been studied in various parts of the mouse body such as the right flank, axilla, and breast. Other sites, such as the eye or back, are also described in scientific literature as tumor implantation locations [19], [20], [21], [22], [23].

Since the implantation of the cells, tumors were of similar size and the implantation in the back was chosen as a suitable site for laser irradiation in our experimental design. Tumors were induced at this site in a sample size of n=3 animals. Tumor size measurements were performed at different time points (4, 7, 11, 15, 23 days) after cell implantation to track tumor size over time. The results are shown on Fig.1. Significant differences in tumor size are observed starting at 7 days as the tumor size increases. At 7 days, the tumor typically exceeds 5 mm in diameter, and at 15 days, it exceeds 10 mm in diameter. Twenty-three days after tumoral cell injection, the tumor is considered too large to assess subtle changes in size and is designated as the termination day for all subsequent experiments.

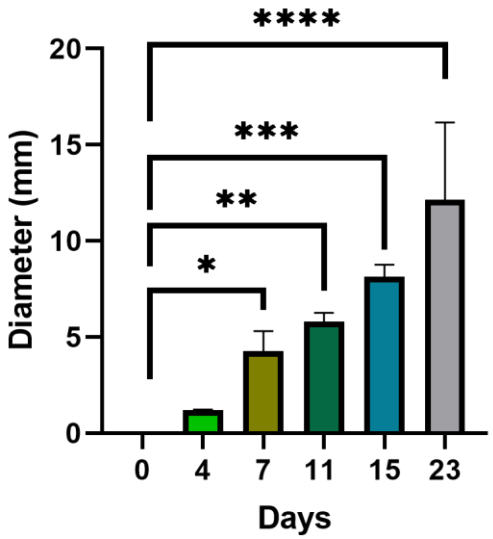

Fig 1: Evolution of tumor size of B16F10 melanoma cells in C57/BL-6 mice at different time points (4, 7, 11, 15 and 23 days) measured by an electronic caliper. p<0.05, **p<0.01, ***p<0.001 ****p<0.0001.

B. PTT in C57/BL-6 melanoma model

A PTT experiment was performed with a sample size of N=6, dividing the animals into the control group and the PTT group, both randomized. PTT is performed 7 days after injection of B16F10 cells. It was observed that the behavior and growth of the melanoma tumor is exactly the same (Fig. 2). In addition to evaluating the diameter of the tumor mass, at the end of the experiment, the tumor is dissected, and the tumor mass is weighed as another method of evaluating the efficacy of PTT, as shown in Fig. 2. The results obtained show significant differences between the control group and the PTT group in both tumor diameter (Fig. 2) and tumor weight (Fig. 3).

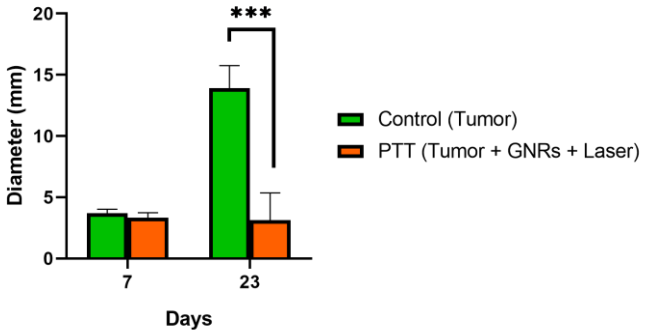

Fig. 2: Tumor diameters in control and PTT-treated C57/BL-6 mice measured 7 (when PTT is applied) and 23 days after the injection of B16F10 cells. ***p<0.001.

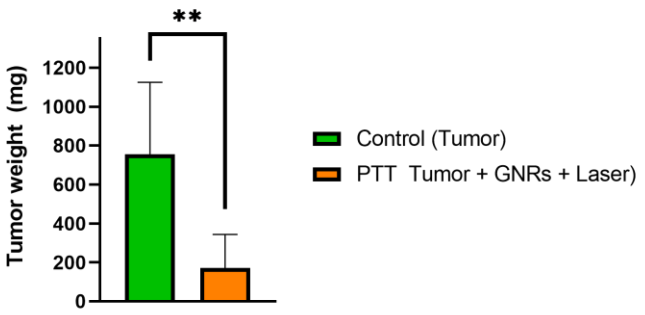

Fig. 3: Weight of dissected tumors obtained from control and PTT-treated C57BL/6 mice, 23 days after injection of B16F10 cells. ***p<0.001.

IV. Discusion

After characterizing the evolution of the tumor over time at different time points (4, 7, 11, 15 and 23 days) after the injection of 100,000 B16F10 cells (Fig. 1), the application of PTT was set one week after cell implantation, when the tumor reached a diameter of approximately 5 mm. Based on the diameter of the tumor, it can be classified as small (<3 mm in diameter), medium (3-15 mm in diameter), and large (>15 mm in diameter). A large melanoma tumor is associated with high mortality, i.e. low survival, and a high probability of metastasis to other organs of the body, such as the liver or lung [24]. In our model, the tumor size in some animals has large dimensions (>15mm) 23 days after cell injection, therefore it was decided not to exceed this time point in any of the studies. The tumor is characterized by high vascularity, highly hemorrhagic and encapsulation. Melanoma cells form diverse architectural patterns including nests, whorls, trabeculae, sheets, nodules, rosettes, glands and papillary formations. They undergo Schwannian, fibroblastic, myofibroblastic, rhabdoid, osteoid, cartilaginous, ganglionic, and smooth muscle differentiation [25]. Immunohistochemical staining is widely used to differentiate melanomas, such as primary melanoma or nevoid melanoma [26].

Once the tumor model was established, PTT was applied for 25 minutes at 450 mW immediately after the injection of GNRs and for a single day. With a single application of PTT, in small tumors (<3mm) grown for 4 days, the tumor disappears, leaving a small scar (data not shown). This is in agreement with other studies found in the literature, such as the work of Pandesh *et al* [27], in which they treat tumors of large volume (100 mm^3) by irradiation for 6 minutes, but with the laser irradiation at a power of 2.5 W/cm^2 (a power much higher than that used in this work.) and using NPs composed of iron oxide with a gold core. In the study by Pandesh *et al*, the tumor is located in the right flank and a drastic tumor shrinkage is achieved.

However, when PTT is performed on medium-sized tumors (<15 mm), the tumor does not disappear, although it does not proliferate as much as the control (untreated), as can be seen in Fig. 2.

According to the literature, the number of NPs injected for tumor treatment, as well as the power and irradiation time, varies depending on the study, as can be found in the scientific literature. Ideally, a low dose of NPs and low laser power should be used along with a reduction in irradiation time. The GNRs used in the PTT experiments are coated with PEG, and the next step after optimization and standardization of the murine melanoma model and establishing the PTT parameters, should be targeted therapy. Strategies in the application of PTT are diverse, including its combination with immunotherapy or the use of nanocomposites [28]. In the study by Balakrishnan *et al* [29]; they use Prussian Blue conjugated NPs injected into the tumor and immediately irradiated for 10 minutes, testing different potencies (0.75, 1, 1.5 and 2W). Subsequently, 5 doses of anti-CD37 antibody or antibodies against immunomodulatory checkpoints such as anti-PD-L1 and CTLA4 are injected. They induce an immunogenic response by filtering out cytotoxic CD8+ T lymphocytes and systemic activation of dendritic cells and T lymphocytes with immunologic memory. Another example is the functionalization of polydopamine in NPs in the tumor located on the back irradiated for 5 minutes at 1.8 W/cm^2 and three doses of these NPs as in the work of Chen *et al* [30]. Therefore, results of a great disparity of parameters and strategies to eliminate the melanoma tumor are found.

In our case, small and medium-sized tumors were treated with a low irradiation dose (450 mW) for 25 min in a single session after injecting a dose of GNRs. The results are promising, and the optimization of the murine melanoma model is complete, although the behavior of biofunctionalized GNRs with molecules that specifically recognize tumor cells remains to be established.

V. Conclusion

This brief but original study in melanoma animal models suggests that PTT is able to completely eliminate tumors when applied to small tumors (2 mm in diameter). In contrast, PTT treatment of larger diameter tumors (4.5 mm) was observed to reduce the rate of tumor growth compared to untreated animals. Further research in this area is fully necessary.

References

[1] S. Strashilov and A. Yordanov, "Aetiology and pathogenesis of cutaneous melanoma: Current concepts and advances," *Int J Mol Sci*, vol. 22, no. 12, Jun. 2021, doi: 10.3390/ijms22126395.

[2] D. E. Brănişteanu *et al.*, "New Treatment Horizons in Uveal and Cutaneous Melanoma," *Life*, vol. 13, no. 8. Multidisciplinary Digital Publishing Institute (MDPI), Aug. 01, 2023. doi: 10.3390/life13081666.

[3] D. Kohoutova, D. Worku, H. Aziz, J. Teare, J. Weir, and J. Larkin, "Malignant melanoma of the gastrointestinal tract: Symptoms, diagnosis,

and current treatment options," *Cells*, vol. 10, no. 2. MDPI, pp. 1–10, Feb. 01, 2021. doi: 10.3390/cells10020327.
[4] D. K. DePalo, K. M. Elleson, M. J. Carr, P. E. Spiess, and J. S. Zager, "Genitourinary melanoma: An overview for the clinician," *Asian Journal of Urology*, vol. 9, no. 4. Editorial Office of Asian Journal of Urology, pp. 407–422, Oct. 01, 2022. doi: 10.1016/j.ajur.2022.01.003.
[5] J. Steininger *et al.*, "Leptomeningeal Metastases in Melanoma Patients: An Update on and Future Perspectives for Diagnosis and Treatment," *International Journal of Molecular Sciences*, vol. 24, no. 14. Multidisciplinary Digital Publishing Institute (MDPI), Jul. 01, 2023. doi: 10.3390/ijms241411443.
[6] S. Santourlidis *et al.*, "Epigenetics in the Diagnosis and Therapy of Malignant Melanoma," *International Journal of Molecular Sciences*, vol. 23, no. 3. MDPI, Feb. 01, 2022. doi: 10.3390/ijms23031531.
[7] G. C. Leonardi *et al.*, "Cutaneous melanoma: From pathogenesis to therapy (Review)," *International Journal of Oncology*, vol. 52, no. 4. Spandidos Publications, pp. 1071–1080, Apr. 01, 2018. doi: 10.3892/ijo.2018.4287.
[8] D. Meng, S. Yang, Y. Yang, L. Zhang, and L. Cui, "Synergistic chemotherapy and phototherapy based on red blood cell biomimetic nanomaterials," *Journal of Controlled Release*, vol. 352. Elsevier B.V., pp. 146–162, Dec. 01, 2022. doi: 10.1016/j.jconrel.2022.10.019.
[9] M. Overchuk, R. A. Weersink, B. C. Wilson, and G. Zheng, "Photodynamic and Photothermal Therapies: Synergy Opportunities for Nanomedicine," *ACS Nano*, vol. 17, no. 9. American Chemical Society, pp. 7979–8003, May 09, 2023. doi: 10.1021/acsnano.3c00891.
[10] J. Estelrich and M. Antònia Busquets, "Iron oxide nanoparticles in photothermal therapy," *Molecules*, vol. 23, no. 7. MDPI AG, 2018. doi: 10.3390/molecules23071567.
[11] Ahmad, T.; Sarwar, R.; Iqbal, A.; Bashir, U.; Farooq, U.; Halim, S.A.; Khan, A.; Al-Harrasi, A. Recent advances in combinatorial cancer therapy via multifunctionalized gold nanoparticles. Nanomedicine **2020**, 15, 1221–1237.
[12] Casanova-Carvajal, O.; Urbano-Bojorge, A.L.; Ramos, M.; Serrano-Olmedo, J.J.; Martinez-Murillo, R. Slowdown intracranial glioma progression by optical hyperthermia therapy: Study on a CT-2A mouse astrocytoma model. Nanotechnology 2019, 30, 355101.
[13] Gonçalves, D.P.N.; Park, D.M.; Schmidt, T.L.; Werner, C. Modular peptide-functionalized gold nanorods for effective glioblastoma multicellular tumor spheroid targeting. Biomater. Sci. 2018, 6, 1140–1146
[14] Jenkins, S.V.; Nedosekin, D.A.; Miller, E.K.; Zharov, V.P.; Dings, R.P.M.; Chen, J.; Griffin, R.J. Galectin-1-based tumour-targeting for gold nanostructure-mediated photothermal therapy. Int. J. Hyperth. 2017, 34, 19–29.
[15] Graczyk, A.; Pawlowska, R.; Jedrzejczyk, D.; Chworos, A. Gold Nanoparticles in Conjunction with Nucleic Acids as a Modern Molecular System for Cellular Delivery. Molecules 2020, 25, 204.
[16] Thi, T.T.H.; Pilkington, E.H.; Nguyen, D.H.; Lee, J.S.; Park, K.D.; Truong, N.P. The Importance of Poly (Ethylene Glycol) Alternatives for Overcoming PEG Immunogenicity in Drug Delivery and Bioconjugation. Polymers 2020, 12, 298.
[17] H Maeda, J. Wu, T. Sawa, Y. Matsumura, and K. Hori, "Tumor vascular permeability and the EPR effect in macromolecular therapeutics: a review a , a a b c," 2000.
[18] González-Rubio, S.; Salgado, C.; Manzaneda-González, V.; Muñoz-Úbeda, M.; Ahijado-Guzmán, R.; Natale, P.; AlmendroVedia, V.G.; Junquera, E.; Barcina, J.O.; Ferrer, I.; et al. Tunable gold nanorod/NAO conjugates for selective drug delivery in mitochondria-targeted cancer therapy. Nanoscale 2022, 14, 8028–8040.
[19] A. Chakraborty, G. Roy, F. Fatima, B. Swami, and S. Bhaskar, "Mycobacterium indicus pranii therapy suppresses systemic dissemination of tumor cells in B16F10 murine model of melanoma," *Biomedicine and Pharmacotherapy*, vol. 160, Apr. 2023, doi: 10.1016/j.biopha.2023.114307.
[20] E. Stoyanova *et al.*, "Antitumor Properties of Epitope-Specific Engineered Vaccine in Murine Model of Melanoma," *Mar Drugs*, vol. 20, no. 6, Jun. 2022, doi: 10.3390/md20060392.
[21] Y. yuan Wang, S. ying Li, S. qian Chen, L. liang Wang, and Z. qiang Han, "Myeloid-derived Suppressor Cells Activate Liver Natural Killer Cells in a Murine Model in Uveal Melanoma," *Curr Med Sci*, vol. 42, no. 5, pp. 1071–1078, Oct. 2022, doi: 10.1007/s11596-022-2623-3.
[22] J. Wang *et al.*, "Post-irradiation intratumoral heterogeneity modulates response to immune checkpoint inhibition therapy in a murine melanoma model," *Neoplasia (United States)*, vol. 36, Feb. 2023, doi: 10.1016/j.neo.2022.100864.
[23] T. Numata, S. Kiryu, T. Maeda, C. Egusa, R. Tsuboi, and K. Harada, "A pulmonary metastatic model of murine melanoma assessed by magnetic resonance imaging," *Experimental Dermatology*, vol. 26, no. 7. Blackwell Publishing Ltd, pp. 619–621, Jul. 01, 2017. doi: 10.1111/exd.13327.
[24] E. E. Nichols, A. Richmond, and A. B. Daniels, "Tumor Characteristics, Genetics, Management, and the Risk of Metastasis in Uveal Melanoma," *Seminars in Ophthalmology*, vol. 31, no. 4. Taylor and Francis Ltd, pp. 304–309, Jul. 03, 2016. doi: 10.3109/08820538.2016.1154175.
[25] S. S. Banerjee and M. Harris, "Morphological and immunophenotypic variations in malignant melanoma," *Histopathology*, vol. 36, no. 5. pp. 387–402, 2000. doi: 10.1046/j.1365-2559.2000.00894.x.
[26] S. J. Ohsie, G. P. Sarantopoulos, A. J. Cochran, and S. W. Binder, "Immunohistochemical characteristics of melanoma," *Journal of Cutaneous Pathology*, vol. 35, no. 5. pp. 433–444, May 2008. doi: 10.1111/j.1600-0560.2007.00891.x.
[27] S. Pandesh, S. Haghjooy Javanmard, A. Shakeri-Zadeh, and P. Shokrani, "Targeted photothermal therapy of melanoma in C57bl/6 mice using Fe3 O4 @Au core-shell nanoparticles and near-infrared laser," *J Biomed Phys Eng*, vol. 11, no. 1, pp. 29–38, 2021, doi: 10.31661/jbpe.v0i0.736.
[28] E. Soratijahromi, S. Mohammadi, R. Dehdari Vais, N. Azarpira, and N. Sattarahmady, "Photothermal/sonodynamic therapy of melanoma tumor by a gold/manganese dioxide nanocomposite: In vitro and in vivo studies," *Photodiagnosis Photodyn Ther*, vol. 31, Sep. 2020, doi: 10.1016/j.pdpdt.2020.101846.
[29] P. B. Balakrishnan *et al.*, "CD137 agonist potentiates the abscopal efficacy of nanoparticle-based photothermal therapy for melanoma," *Nano Res*, vol. 15, no. 3, pp. 2300–2314, Mar. 2022, doi: 10.1007/s12274-021-3813-1.
[30] W. Chen, M. Qin, X. Chen, Q. Wang, Z. Zhang, and X. Sun, "Combining photothermal therapy and immunotherapy against melanoma by polydopamine-coated Al 2 O 3 nanoparticles," *Theranostics*, vol. 8, no. 8, pp. 2229–2241, 2018, doi: 10.7150/thno.24073.